Published by IOP Publishing for Sissa Medialab

Received: *December 11, 2023*
Revised: *February 13, 2024*
Accepted: *March 18, 2024*
Published: *May 7, 2024*

16th Topical Seminar on Innovative Particle and Radiation Detectors
Siena, Italy
25–29 September 2023

High granularity resistive Micromegas for tracking detectors in future experiments

M.T. Camerlingo,[a,*] **M. Alviggi**,[a,b] **M. Biglietti**,[c] **M. Della Pietra**,[a,b] **R. Di Nardo**,[c,d] **P. Iengo**,[a] **M. Iodice**,[c] **F. Petrucci**,[c,d] **G. Sekhniaidze**[a] **and M. Sessa**[e]

[a] *INFN Section of Napoli, Via Cinthia 26, Napoli 80126, Italy*
[b] *Università degli studi di Napoli "Federico II", Via Cinthia 26, Napoli 80126, Italy*
[c] *INFN Section of Roma Tre, Via della Vasca Navale 84, Roma 00146, Italy*
[d] *Università degli Studi di Roma Tre, Via della Vasca Navale 84, Roma 00146, Italy*
[e] *INFN Section of Roma Tor Vergata, Via della Ricerca Scientifica 1, Roma 00133, Italy*

E-mail: maria.teresa.camerlingo@cern.ch

Abstract: After exploring different solutions and testing several options, the high granularity resistive Micromegas technology is now mature enough to offer an efficient operation up to particle rates of 10 MHz/cm^2, maintaining the gas amplification above 10^4, with a large margin before breakdown in order to ensure a stable and reliable operation. The detector exploits small-size readout pads for occupancy reduction and a double Diamond-Like Carbon (DLC) resistive layer with a network of dot-connections to ground for a fast charge evacuation. The double-layer allows preserving the minimum resistance to suppress the discharge intensity for stable operations. The performance measured with particle beams at CERN have shown a spatial resolution below 100 µm for mm-wide readout pads and a few ns time resolution. Now, the technology is being scaled to larger areas, with the construction of detectors with an active area of ~20×20 cm^2 (already achieved) and new ~40×50 cm^2 prototypes under construction. An overview of the detector technology, including the latest results, is presented in terms of the gain and rate capability (measured in the laboratory) and efficiency, time and spatial resolution (measured at the CERN SPS). Possible applications in HEP experiments, as well as future developments, are also reported.

Keywords: Micropattern gaseous detectors (MSGC, GEM, THGEM, RETHGEM, MHSP, MICROPIC, MICROMEGAS, InGrid, etc); Particle tracking detectors (Gaseous detectors)

*Corresponding author.

https://doi.org/10.1088/1748-0221/19/05/C05004

Contents

1 Introduction

The high granularity resistive Micromegas detector [1] is a quite novel technology for tracking in future experiments. It matches the standard Micromegas layout with a pad readout geometry and customised spark-protection resistive structure. A standard Micromegas detector [2] is a single-stage amplification gaseous detector based on a parallel plate electrode structure. The gas volume is divided into two gaps using a stainless steel micro-mesh. Two different electric fields are applied in the gaps. The region between the mesh and the cathode plane (the conversion and drift gap) is a few mm deep, and the other gap between the mesh and the anode plane (the amplification gap) is about 0.1 mm deep, with the anode hosting the readout elements, usually micro-strips. Under intense particle fluxes, discharge effects are greatly mitigated by implementing a layer of resistive strips facing the amplification gap [3]. This is the solution developed, and already applied, by ATLAS for operations up to tens kHz/cm^2 [4]. To efficiently operate at the foreseen future rates, the Resistive High granUlarity Micromegas (RHUM) project [5] proposes resistive Micromegas detectors with readout pads of few mm^2 that assure the proper occupancy. The resistive structures of RHUM detectors share the same quenching principle of the resistive strips of ATLAS Micromegas detectors. However, new designs with two planes of resistive elements were adopted for the recent pad geometry and higher rates, aiming at a stable behaviour at a high gain factor, simple construction technique and spatial and time resolution below 100 µm and below 10 ns, respectively. The project started in 2015 with the idea to propose the resistive Micromegas detectors for a high−η tagger for ATLAS [6]. Over time, we effectively aim to develop versatile detectors that can be customised according to the application in the context of future HEP experiments. To reach these goals, an effort was made to optimise this layout and construction technique [7] during the early times of the project. The second phase was focused on the rate capability and stability studies and, at the moment, we are launching the construction of large surface detectors and studying the tracking and timing performance in more details.

2 Resistive High granUlarity Micromegas project

Two different classes of spark-protective resistive schemes were implemented for the pad readout geometry. The first presents independent embedded protective resistors for each readout pad (sketched

2024 JINST 19 C05004

on the left side of figure 1). The most recent scheme (represented on the right of figure 1) consists of two resistive planes crossed by dot-connections to the ground (evacuation vias). The used resistive materials are: carbon paste and segmented Diamond-Like-Carbon (DLC) for the first class (according to the prototype), and the DLC for the second scheme class. In both classes, the double-layer design makes the resistance between the top layer and the ground homogeneous. The three prototypes featured

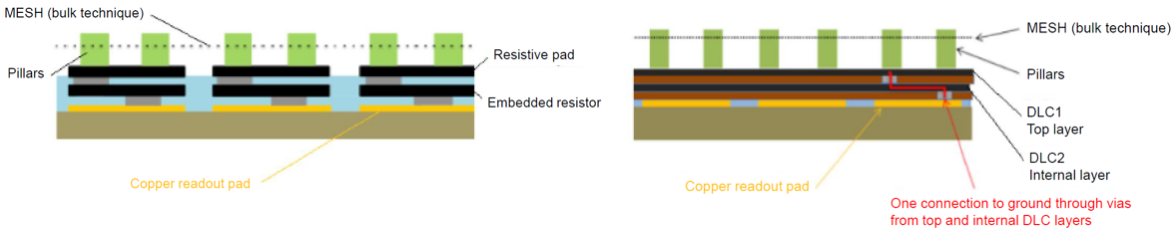

Figure 1. A sketch of the Micromegas PCB with the resistive scheme with pad-patterned embedded resistors (on the left) and one with the DLC double-layer scheme (on the right).

in this proceeding mount the second scheme class, i.e. the DLC double-layer scheme. They are named DLC-20, SBU-3 and Paddy400, and their relevant parameters are reported in table 1. The DLC-20 is one of the first prototypes and a reference to compare with newer detectors. The SBU-3 was built using the updated construction technique that includes Sequential Build-Up (SBU) technology [8] in the manufacture of the DLC double-layer structure. The Paddy400 is the first middle-size prototype. It has a ~20×20 cm^2 area and readout pads with 1×8 mm^2 size, for a total of 4800 readout channels. It implements the DLC double-layer scheme with an 8 mm vias pitch. The measured DLC resistivity is 26 MΩ/□ for the top/external DLC layer (close to the gas gap) and 34 MΩ/□ for the bottom/inner layer, respectively. In table 1, the resistivity is reported in a more compact way using the average value of the two layers. The transverse section of a complete detector is represented in figure 2, where the typical elements of a Micromegas chamber are pointed out, like micro-mesh, amplification and drift gaps (defined in section 1). The typical electric field magnitude is a few hundred V/cm in the drift region. A more intense electric field of 40–50 kV/cm magnitude is applied in the thin amplification region. More specifically, the present detectors were made using the Micromegas-bulk technique [2], in which the micro-mesh is bulked in a dielectric material that was finally subjected to an etching process to realise dielectric spacers, referred to as Micromegas's pillars. These pillars assure the uniformity of the amplification electric field by homogenising the distance between the micro-mesh and resistive structure. Paddy400's pillar diameter is 800 µm. Finally, the drift gap of all detectors is 5 mm.

Table 1. Parameters of the three tested detectors. Nominal resistivity (*) is the average of the two DLC layers. The vias pitch (**) is 6 mm in a half side of the DLC-20 chamber and, in its other side, the vias pitch is 12 mm.

Parameter	Paddy400	DLC-20	SBU-3
Area (cm^2)	20×20	4.8×4.8	4.8×4.8
Pad size (mm^2)	1×8	1×3	1×3
Drift gap (mm)	5	5	5
Nominal resistivity(*) (MΩ/□)	30	20	30
Pillar diameter (µm)	800	300	800
Vias pitch (mm)	8	6 and 12 (**)	6

2024 JINST 19 C05004

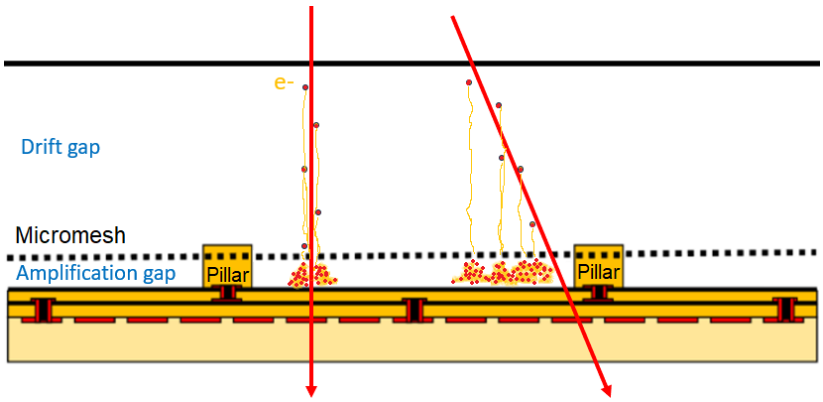

Figure 2. A sketch of the transverse section of a resistive Micromegas with the DLC double-layer scheme. It is not in scale. The depth of the amplification (drift) gap is 0.12 mm (5 mm).

3 Rate capability

Studies of the rate capability were carried out using an X-ray gun with a Cu target at the CERN GDD Laboratory [9]. The active area was covered by a Cu mask of few mm thickness with a 10 mm diameter circular opening. The applied X-ray gun voltage was set to extract photons of 8 keV energy from the target, while the X-ray gun current was varied to perform a X-ray intensity scan. Figure 3 shows the gain as a function of the hit rate. For these results, the hit rate is derived using the extrapolation of the linear regression between the X-ray gun current and hit rates below 300 kHz, which can be directly measured. Looking at figure 3, the gain is stable up to 1–2 MHz/cm^2. In the range of higher rates, the gain drop (due to the ohmic contribution) is visible but still limited. At 10 MHz/cm^2 rate, it is about 20%, and an increase of 10 V in amplification voltage can compensate it. Two different gaseous mixtures were studied, Ar:CO_2(93:7) and Ar:CO_2:iC_4H_{10}(93:5:2). The relative trends are similar for the two mixtures (visible in figure 3), but the addition of 2% of isobutane produces higher gain and quenching.

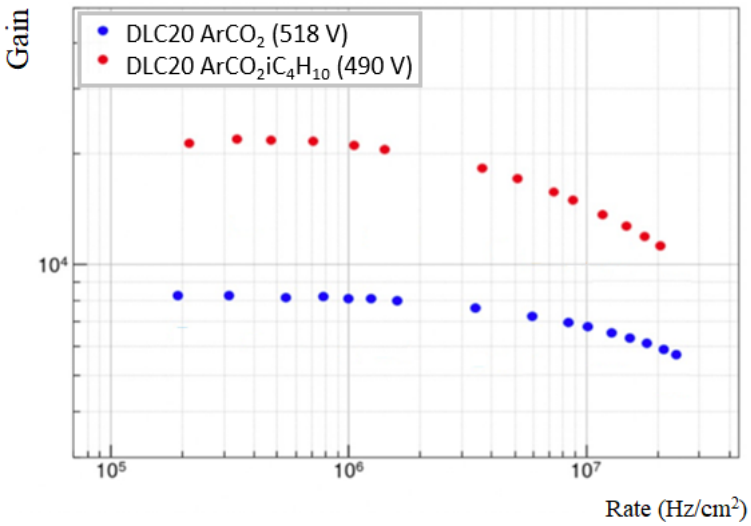

Figure 3. The DLC-20 gain as a function of the hit rate for Ar:CO_2(93:7) in blue and Ar:CO_2:iC_4H_{10}(93:5:2) in red.

2024 JINST 19 C05004

4 Tracking and timing studies at CERN SPS H4 beam line

The tracking performance were tested at the CERN SPS H4 beam line [10] with 150 GeV/c muons. The three prototypes (DLC-20, SBU-3 and Paddy400) were mounted in a tracker telescope[1] (in figure 4), equipped with a fourth pad detector, used as the reference in the time studies, a trigger system and an independent tracking system. Two scintillating counters, in coincidence, formed the telescope trigger system. The telescope tracking system had two resistive strip Micromegas detectors with 2D strip readout to locate the track extrapolations inside the prototypes under test. The gaseous mixture is

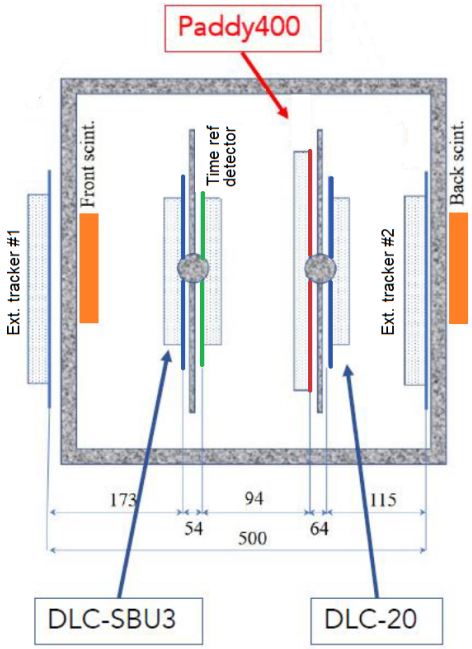

Figure 4. The scheme of the test beam tracker telescope. In this scheme, the configuration at the 0° incident angle corresponds to the case when the beam is perpendicular to the tracking planes of the detectors. The distances are in mm.

Ar:CO_2:iC_4H_{10}(93:5:2). The studied dataset contains the events where one cluster is reconstructed in each external tracker, and their number defines the denominator in the estimate of the efficiency. The successful events include the cases where one cluster is inside the fiducial interval of 1.5 mm around the extrapolated x position in the analysed prototype. On the left side of figure 5, the low-efficiency spots correspond to the positions where the dielectric pillars (defined in section 2) are. Outside the regions covered by pillars, the efficiency is close to 1. On the right side of figure 5, the average efficiency over the tracking plane is represented as a function of the gain factor, and the plateaux are observed for gains larger than 5000 with asymptotic values of $\sim 96 \div 97\%$.

After removing the condition on the fiducial interval of the extrapolated position, the spatial resolution along the x coordinate with the finest pad granularity is studied as a function of the gain. The tails in the residual distributions are negligible with respect to their core, as visible in the left side of figure 6. Then, for this study, the spatial resolution is evaluated from the core standard deviation,

[1]The mechanical structure can rotate the detectors with respect to the beam. Data at large incident angles were acquired. However, their analysis is still ongoing. Then, all the results are relative to the 0° incident angle configuration.

2024 JINST 19 C05004

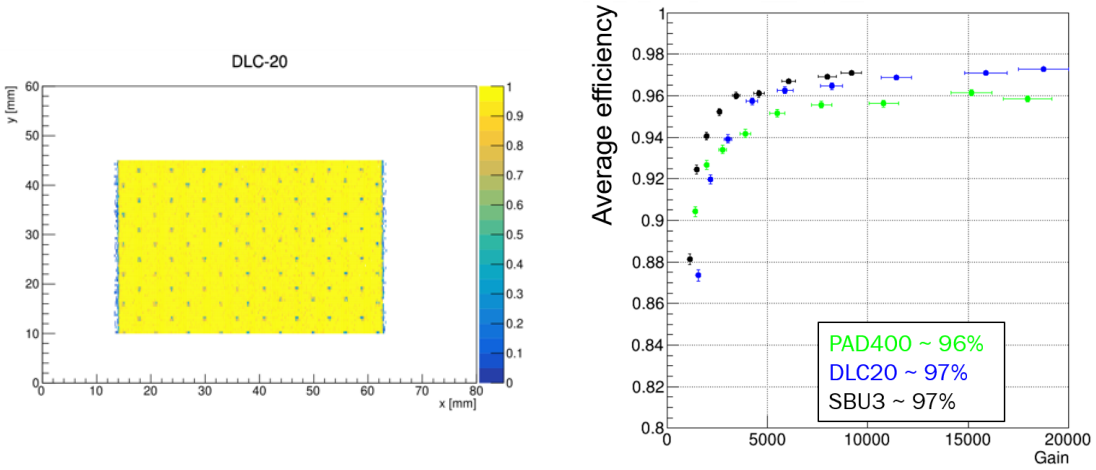

Figure 5. Left: an example of an efficiency map, relative to DLC-20 prototype, Ar:CO_2:iC_4H_{10}(93:5:2), V_{ampl} = 440 V (gain is ~ 4k) and E_{drift} = 500 V/cm. Right: The efficiency as a function of the gain with the Ar:CO_2:iC_4H_{10}(93:5:2) and E_{drift} = 600 V/cm for the three detectors. A fiducial interval is set 1.5 mm around the extrapolated x position along the direction with the finest pad granularity.

resulting from the fit with a double gaussian function. In the right side of figure 6, the contribution of the uncertainty of the track extrapolation (ranging between 50–60 µm) is subtracted in quadrature from the core standard deviation of the distribution of the residuals. These figures show the results of the dataset with Ar:CO_2:iC_4H_{10}(93:5:2) and drift electric field 600 V/cm for the three cited prototypes. In the investigated range of the gain, the spatial resolution reaches values smaller than 100 µm along the x coordinate with 1 mm pitch. For the DLC-20, the best value is 65 µm. These results are excellent first showcases to prove that our detectors are suitable for next-generation experiments.

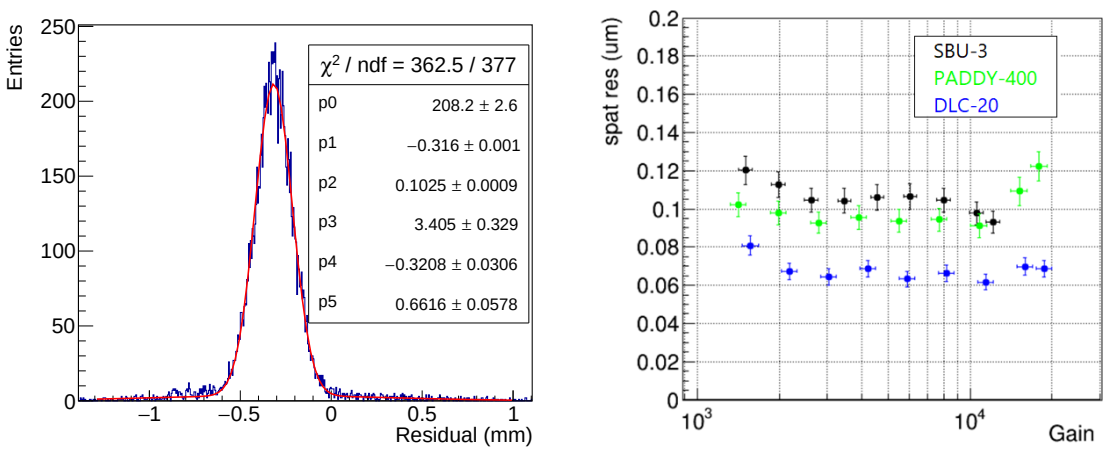

Figure 6. Left: an example of a distribution of the residuals. It is fitted by a double gaussian, and it corresponds to the Paddy400 prototype with gain ~ 8k (V_{ampl} = 460 V) and Ar:CO_2:iC_4H_{10}(93:5:2). In the label $\{p0; p1; p2\}$ are respectively the constant, mean and standard deviation of the core gaussian, while $\{p3; p4; p5\}$ are the corresponding parameters of the tail gaussian. Right: the spatial resolution of the three prototypes as a function of the gain with the Ar:CO_2:iC_4H_{10}(93:5:2) and E_{drift} = 600 V/cm. At the highest gains, the rising trend is due to signals that saturate the ADC channels inside the electronic readout system.

2024 JINST 19 C05004

The timing performance of the detectors has been studied as a function of the electron drift velocity. As expected, the time resolution and the electron drift velocity are strongly correlated since the first is dominated by the spatial distribution of the ionisations along the track of the incoming charged particles in the drift gap. Therefore, the faster the drift velocity, the smaller the dispersion of the arrival times of the drift electrons to the amplification gap. To explore a wide range of the drift velocities, the data were acquired varying the drift electric field and gaseous mixture. Specifically, to achieve the highest velocities, the Ar:CF_4:iC_4H_{10}(88:10:2) mixture was exploited. The used Front-End chip is the APV25 chip [11], read by the SRS system [12]. The signal passes a charge preamplifier and CR-RC shaper. The output of the shaper is sampled at 40 MHz and stored in an analogue pipeline. Finally, it is converted to digital by an ADC external to the APV chip. An example of a single-pad output signal, with a 25 ns sampling, is shown in the left side of figure 7. It keeps information of the signal waveform. Its rise is fitted by a Fermi-Dirac-like function named $f(t)$ in the figure. The parameter T_{FD} of the fit function defines the hit time, equal to the time at half of the signal rise edge. It is used to build a time variable to associate with the reconstructed cluster. Specifically, the shortest time among the hit times that belong to the same reconstructed cluster, the earliest time, is chosen to define the cluster time. Assuming identical detectors and requiring a reconstructed cluster per each chamber, the total time resolution is obtained from the distribution of the difference of the cluster times for each pair of detectors under test using equation (4.1).

$$\sigma_{\mathrm{total}} = \frac{(\sigma_{D1-D2})}{\sqrt{2}} \tag{4.1}$$

As example, the right side of figure 7 shows the distribution of the difference of the cluster times for the pair of Paddy400 and SBU-3 at the highest investigated drift velocity (about 10 cm/µs). By applying equation (4.1) on the results of a fit with a gaussian, the total time resolution of a single detector is 8.8 ± 0.2 ns. The difference of the cluster times cancels the jitter between the start time of the acquisition windows and the arrival time of the asynchronous trigger signal that only enables

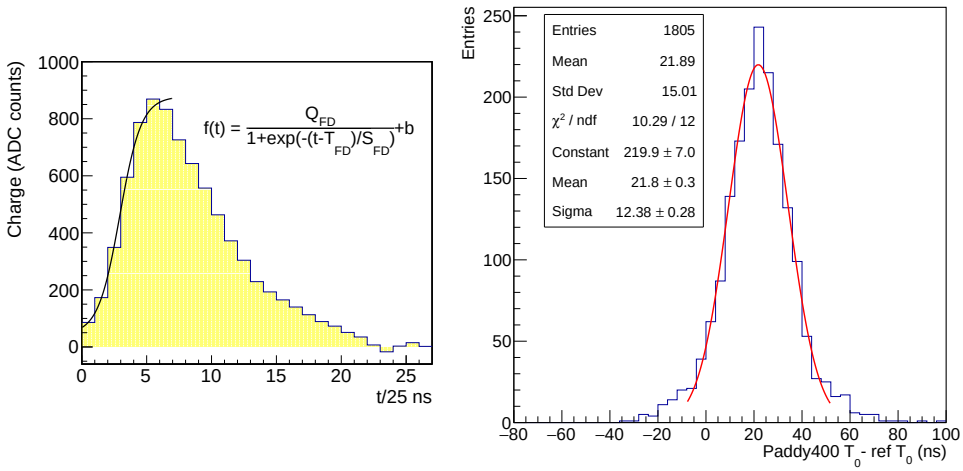

Figure 7. Left: an example of a single-pad signal, sampled in time bins of 25 ns by the FE used during the test beam, on which a Fermi-Dirac-like function fit (black curve) is performed to estimate the time at half of the signal rise. Right: the distribution of the difference between the earliest times of the clusters in the same event in Paddy400 and SBU-3, used as the reference chamber in this case. The distribution is fitted using a gaussian (in red) and its standard deviation *Sigma* is named σ_{D1-D2} in equation (4.1).

2024 JINST 19 C05004

the acquisition. No contributions due to the FE or measurement procedure are subtracted from the measured time resolution. The comparison of the trends as a function of the drift velocity (in figure 8) between different pairs of detectors confirms the assumption that the time performance of the detectors are identical within the measurement uncertainties. As expected, the time resolution improves with a faster gas mixture, as visible in figure 8, in which the red markers represent Ar:CF_4:iC_4H_{10}(88:10:2) mixture, and the blue ones refer to the nominal Ar:CO_2:iC_4H_{10}(93:5:2) mixture. In the complete study, two other different definitions of cluster time are taken into account in addition to the earliest time: the mean time and the charged-weighted time of the cluster. The mean time is the average of the hit times that belong to the same reconstructed cluster, and charged-weighted time is the weighted mean of hit times of a cluster with the hit charge (Q_{FD} in the label on the left side of figure 7) as the weight. Their results will be compared at different incident angles. However, the analysis of the dataset at larger angles than 0° is not concluded. For this reason, only results relative to the earliest time at the 0° incident angle were presented in figure 8. The results of the charged-weighted time at the 0° incident angle can be found in reference [13].

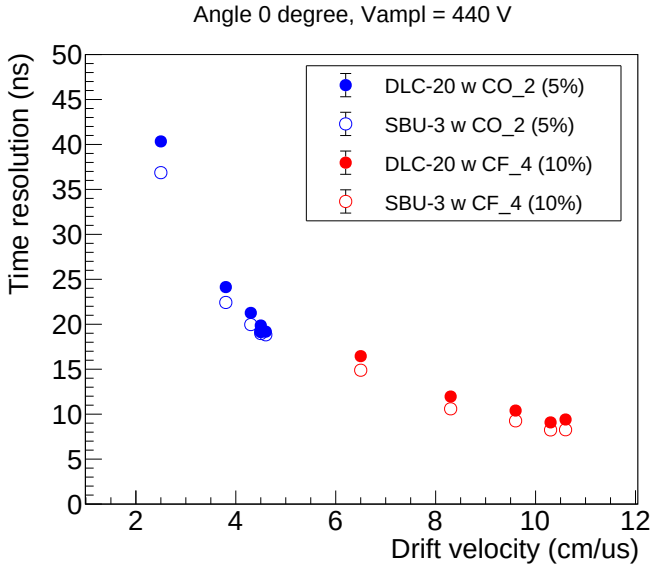

Figure 8. The total time resolution as a function of the drift velocity, evaluated using the earliest time of the cluster. Blue dataset are relative to Ar:CO_2:iC_4H_{10}(93:5:2) and the curves with Ar:CF_4:iC_4H_{10}(88:10:2) are in red. The drift velocity values along the horizontal axis are the simulated values corresponding to the applied drift field. The used simulation software is Magboltz [14] in the Garfieldpp [15] toolkit. No contributions due to the FE or measurement procedure are subtracted from the shown values.

5 Operation in future experiments

The resistive Micromegas detectors, developed by the RHUM project, got the attention of new experiments under proposal or upgrade. The Shadows experiment [16] is a newly-proposed proton beam dump experiment placed off-axis in the ECN3/TCC8 experimental cavern at CERN to search for feebly-interacting particles. Its collaboration intends to use the resistive Micromegas with pad readout as its Upstream muon Veto. Considering the expected incident rate, a DLC single-layer solution is also under evaluation to simplify and reduce the costs. The spatial resolution requests drive the readout

2024 JINST 19 C05004

pad segmentation. They can be fulfilled by $1\times1\,cm^2$ square pads. The design foresees a configuration with two independent tracking layers with pad readout to maximize the detector performances. The expected combined efficiency is $\sim$ 99%, and the spatial and time resolutions improve by a factor $\sqrt{2}$ when the muon is detected by both tracking layers.

The AMBER [17] collaboration is evaluating to replace its multiwire chambers with resistive Micromegas detectors in its Muon system.

The shown interest did not limit to possible tracking applications of our detectors. Indeed, a new R&D [18] started, and it is testing some resistive Micromegas prototypes with pad readout to develop a digital and semidigital hadronic calorimeter based on MPGD detectors.

6 Conclusions

In conclusion, the R&D project is in an advanced status. Indeed, some new experiments and other R&D collaborations showed interest in the RHUM prototypes. The presented results highlight that small-Pad resistive Micromegas detectors are suitable candidates for the particle tracking and trigger operation in next-generation experiments, with a margin of improvement with customised optimisations and different electronics. They have already proved to have a stable HV behaviour, below 100 µm spatial resolution for perpendicular tracks, and below 10 ns total time resolution. The constructive technique is consolidated to the point that a $\sim40\times50\,cm^2$ detector is under realisation.

Acknowledgments

We would like to thank the CERN MPT Workshop for the design and construction of the detector and the colleagues of the RD51 Collaboration for the support during the tests at the GDD Laboratory and at the H4 SPS beam line.

References

[1] M. Alviggi et al., *Construction and test of a small-pad resistive Micromegas prototype*, 2018 *JINST* **13** P11019.

[2] I. Giomataris et al., *Micromegas in a bulk*, *Nucl. Instrum. Meth. A* **560** (2006) 405 [physics/0501003].

[3] T. Alexopoulos et al., *A spark-resistant bulk-micromegas chamber for high-rate applications*, *Nucl. Instrum. Meth. A* **640** (2011) 110.

[4] T. Kawamoto et al., *New Small Wheel Technical Design Report*, CERN-LHCC-2013-006 (2013).

[5] M. Alviggi et al., *High granularity small-pad resistive micromegas for rates above MHz/cm2*, *Nucl. Instrum. Meth. A* **1048** (2023) 167944.

[6] ATLAS collaboration, *Technical Design Report for the Phase-II Upgrade of the ATLAS Muon Spectrometer*, CERN-LHCC-2017-017 (2017).

[7] M. Iodice et al., *Small-Pad Resistive Micromegas: rate capability for different spark protection resistive schemes*, 2020 *JINST* **15** C09043.

[8] https://hdihandbook.com/index.php.

[9] https://gdd.web.cern.ch.

2024 JINST 19 C05004

[10] https://home.cern/science/accelerators/super-proton-synchrotron.

[11] M.J. French et al., *Design and results from the APV25, a deep sub-micron CMOS front-end chip for the CMS tracker*, *Nucl. Instrum. Meth. A* **466** (2001) 359.

[12] S. Martoiu, H. Muller, A. Tarazona and J. Toledo, *Development of the scalable readout system for micro-pattern gas detectors and other applications*, 2013 *JINST* **8** C03015.

[13] M. Iodice et al., *Towards large size pixelized Micromegas for operation beyond 1 MHz/cm^2*, 2023 *JINST* **18** C06029.

[14] S. Biagi, *Magboltz*, https://magboltz.web.cern.ch/magboltz.

[15] H. Schindler and R. Veenhof, *Garfield++*, https://garfieldpp.web.cern.ch/garfieldpp.

[16] SHADOWS collaboration, *SHADOWS Technical Proposal*, CERN-SPSC-2023-029 (2023).

[17] M.G. Alexeev et al., *Development of a Micromegas prototype for the AMBER experiment at CERN*, *Nucl. Instrum. Meth. A* **1049** (2023) 168043.

[18] Muon Collider Physics and Detector Group collaboration, *Design and simulation of a MPGD-based hadronic calorimeter for Muon Collider*, *Nucl. Instrum. Meth. A* **1047** (2023) 167731.

2024 JINST 19 C05004